Tunable UV spectrometer for Doppler broadening thermometry of mercury

Abstract

We realised a UV laser spectrometer at 253.7 nm for Doppler-broadening thermometry on the $^1S_0$-$^3P_1$ intercombination line in mercury vapors. Our setup is based on the two-stage duplication of a 1014.8 nm diode laser in a fiber-coupled periodically-poled lithium niobate waveguide crystal and a beta-barium borate crystal in enhancement cavity, and we exploit injection locking of a 507.4 nm diode laser to boost the available optical power after the first duplication. Our setup addresses spectroscopic features which allow the thermodynamic temperature determination of the atomic sample from the absorption profile with 10^{-6} accuracy. The realized UV laser source has 1×10^{-4} relative intensity stability, Gaussian shape and over 10 GHz mode-hop-free tunable range. These features are crucial for the practical realization of the kelvin in the new International System of Units through a spectroscopic technique.

A tunable UV spectrometer for Doppler broadening thermometry of mercury

Cecilia Clivati[1,*], Stefania Gravina[2], Antonio Castrillo[2], Giovanni A. Costanzo[1,3], Filippo Levi[1], and Livio Gianfrani[2]

[1]Istituto Nazionale di Ricerca Metrologica (INRiM), Torino, Italy
[2]Department of Mathematics and Physics, Università degli Studi della Campania "Luigi Vanvitelli", Caserta, Italy
[3]Department of Electronics and Telecommunications, Politecnico di Torino, Torino, Italy
[*]Corresponding author: c.clivati@inrim.it

July 15, 2020

In the new International System of units (SI), the kelvin, unit of measurement of the thermodynamic temperature T, is defined in terms of a fixed value of the Boltzmann constant, $k_B = 1.380\,649 \times 10^{-23}\,\mathrm{J/K}$. Doppler Broadening Thermometry (DBT) is a promising primary method for its practical realization [1, 2], although it has not yet reached the same accuracy as acoustic gas thermometry and dielectric-constant gas thermometry [3, 4, 5]. DBT is based on measuring the Doppler width of a spectral line of an atomic or molecular gas sample at the thermodynamic equilibrium [6]. So far, the best results have been achieved probing the near-infrared (NIR) vibration-rotation spectrum of acetylene, with an overall uncertainty of 23 parts per million (ppm) for temperature determinations between the triple point of water and the gallium melting point [7].

Past literature shows a few examples of DBT implementations in which low-pressure alkali-metal vapors such as Rb and Cs atoms [8, 9] have been used as thermometric substance. The current limitations of DBT are likely to be overcome by probing the $6s^2\ {}^1S_0 \rightarrow 6s6p\ {}^3P_1$ intercombination transition in mercury at 253.7 nm, which is normally used for laser cooling [10, 11, 12, 13, 14]. DBT can be performed on both bosonic isotopes ^{200}Hg and ^{202}Hg; the former nearby the triple point of water, the latter at lower temperatures. At the temperature of the triple point of water, the vapor pressure of mercury is sufficiently small to neglect the collisional broadening, but at the same time high enough to allow the observation of the intercombination line with a good signal-to-noise ratio. In addition, thanks to the much simpler structure of the spectrum as compared to that of molecules, the line profile is poorly affected by nearby resonances and quantum interference effects[9, 15]. The Zeeman splitting of the spec-

troscopic line (about 2 MHz) can be avoided by magnetic shielding. Finally, the ratio of the Doppler and natural width of the atomic transition is more favourable for the selected Hg line as compared to that of Rb and Cs, allowing interrogation with a sub-kHz-linewidth laser. These features enable to approach the ppm level in temperature determinations, making DBT a viable method for the realization of the new kelvin.
For the practical implementation of the method, the laser source must feature sub-kHz linewidth and traceability to an absolute frequency reference, continuous tunability over 6 GHz to ensure a sufficiently broad scanning region around the line center, 10^{-4} relative intensity stability and a TEM_{00} mode. On the other hand, few μW of optical power are sufficient. These requirements are more stringent and usually not shared with setups designed for laser cooling [10, 11, 12, 13, 14] and spectroscopy [16, 17, 18] of Hg, and call for dedicated solutions.
Here, we describe the realisation of a laser source for DBT of mercury at 253.7 nm which fulfils these requirements and can be tuned continuously over more than 10 GHz. As a first demonstration, we performed Doppler-limited absorption spectroscopy of the intercombination transition of mercury isotopes, in a natural abundant sample. These measurements are preliminary to the realization of a primary thermometer based on DBT in mercury vapors.
Our setup combines the advantages of cascaded second harmonic generation (SHG) of a 1014.8 nm diode laser with the use of a fiber-coupled periodically-poled lithium niobate (PPLN) crystal and the injection lock of a diode laser at 507.4 nm, which is then further duplicated in a beta-barium borate (BBO) crystal.
A detailed sketch of the experimental apparatus is shown in Fig. 1. The master laser (DL1015) is an anti-reflection (AR) coated diode (Toptica photonics LD-1060-0200-AR-2) emitting in the 960 nm-1060 nm region, mounted in an external cavity about 15 mm long and collimated with an aspheric lens with 6.24 mm focal length. Feedback is provided through a blazed grating with 2400 grooves/mm, which has a diffraction efficiency of 30% at 1014.8 nm when the beam polarization is vertical, namely parallel to the grating lines. About 65 mW of optical power are available at output when pumping with 320 mA. The laser can be tuned via the pump current with a sensitivity of 180 MHz/mA, via the temperature (sensitivity 18 GHz/K), or by tilting the piezo-actuated grating (sensitivity 680 MHz/V).

The first-stage duplication (1014.8 nm→507.4 nm) is performed in a fiber-coupled PPLN crystal in waveguide (NTT), which is a robust, alignment-free solution [19, 20]. About 55% of the optical power is coupled to the crystal by correcting the beam ellipticity, about 2.1, with an anamorphic prism pair (AP). Two optical isolators protect the master laser from backreflections occurring on the crystal facets. For the considered optical power, the measured crystal efficiency is $(1.8 \pm 0.2)\mathrm{W}^{-1}$ and about 3 mW of green light are available at the output. The efficiency is optimised by adjusting the crystal temperature, and decreases by less than 3% when the laser frequency is tuned by 2 GHz, which ensures that no temperature tuning is required to maintain the quasi-phasematch condition during the scan. A dichroic mirror (DM) extracts the unconverted NIR radiation, which will be sent to an optical comb for frequency referencing. The produced radiation at 507.4 nm seeds a diode laser (DL507) at the same wavelength (Nichia NDE4116) [21, 22, 23, 17], boosting the optical power available for the second-stage duplication. The green laser has no AR-coating and exhibits multi-mode

emission, with modes separation of ~ 60 GHz. It produces about 80 mW optical power when pumped with 168 mA. The slave laser is mode-matched to the seeding beam using an aspherical collimation lens with focal length of 6.24 mm and a cylindrical telescope to correct its $\sim$2.2 ellipticity. In this condition, injection lock at the minimum seed power (0.9 mW) is achieved by simply overlapping the beam paths. Raising the seed power to 1.5 mW guarantees stable and single-mode operation for several hours. We detected the beatnote between the seeding beam and the slave laser, this latter shifted with an acousto-optic modulator (AOM), on a spectrum analyzer and ensured that no excess noise was added by the injection lock. The slave laser passes through an AOM which is used to stabilise the power, then it is coupled to a polarization-maintaining optical fiber for mode cleaning, with $>$50% coupling efficiency.

The second duplication (507.4 nm$\rightarrow$253.7 nm) is performed with a BBO crystal (Castech) cut at θ=51.2°, housed in a bow-tie cavity with folding angle $\alpha/2$= 14°. The crystal is AR-coated at 507.4 nm and at 253.7 nm and is 12 mm long. According to the Boyd-Kleyman formula [24], the cavity should be designed with a beam waist of 19 µm in the crystal. However, due to the high walk-off ρ =84.7 mrad of BBO, it is preferable to operate with a larger waist on the horizontal plane. Similarly to what has been described in [18], we designed the cavity [25, 26] to have a waist of 30 µm in the horizontal plane, while on the vertical plane the waist is maintained at its optimal value. The cavity has two plane mirrors (M1 and M2) and two concave mirrors (M3 and M4) with radius 75 mm and is 341 mm long, which leads to a free spectral range of 880 MHz. The input mirror M1 has nominal reflectivity $R_1 = 0.986$, while mirrors M2, M3, M4 have reflectivity $R_2, R_3, R_4 > 0.999$ at 507.4 nm. The fundamental beam is coupled to the secondary waist using a spherical telescope and a cylindrical lens. The BBO crystal is mounted on a rotatable platform for phase-matching optimization and is placed inside an oven. Although birefringent phase-matching is achieved by angle-tuning only, the crystal is temperature-stabilized at 50 °C to prevent water vapour deposition and reduce degradation [18]. The cavity is locked to the incoming beam through the Hänsch-Couillaud technique [27], by moving the piezo-actuated mirror M2. The mechanical resonance of the mirror and piezo system is 20 kHz and the piezo maximum stroke is 6.5 µm. These features enable both to keep a tight lock of the cavity and to follow scans of the 507.4 nm laser frequency as broad as 5 GHz.

The produced UV power was measured on a silicon carbide (SiC) photodiode with a responsivity of 0.08 A/W at 253.7 nm and $< 8 \times 10^{-9}$ A/W at 507.4 nm, which ensures sufficient blindness to stray light at the fundamental wavelength.

In a single pass, the produced UV power P_{SHG} can be expressed in terms of the fundamental power P_{inc} by the quadratic relation $P_{\mathrm{SHG}} = \eta P_{\mathrm{inc}}^2$ where the conversion efficiency η can be calculated by the Boyd and Kleinman formula [24]. By performing a quadratic fit of the produced UV power versus incident power, we estimated an efficiency of $\eta = (5.7 \pm 0.3) \times 10^{-5}\ \mathrm{W}^{-1}$ for the BBO crystal. In an enhancement cavity, the power of the second-harmonic beam can be written in terms of the fundamental as [26]:

$$P_{\mathrm{SHG}} = \eta c_0^2 \frac{(1-R_1)^2}{\left(1-\sqrt{(R_1(1-l_{\mathrm{cav}})}\right)^4} P_{\mathrm{inc}}^2 \tag{1}$$

Here, $l_{\mathrm{cav}} = 1 - R_2 R_3 t_{\mathrm{AR}}^2 \alpha_{507} R_4$ includes all optical losses of the setup except for those due to second-harmonic generation, namely, the reflectivity of cavity mirrors, the transmission t_{AR} on the input and output facets of the BBO crystal at 507.4 nm, and the crystal absorption α_{507}. c_0 represents the mode-matching coefficient and was estimated by comparing the measured ratio $P_{\mathrm{refl}}/P_{\mathrm{inc}}$ of reflected versus incident power with the expected one:

$$\frac{P_{\mathrm{refl}}}{P_{\mathrm{inc}}} = \frac{\sqrt{R_1} - \sqrt{1 - l_{\mathrm{cav}}}}{\left(1 - \sqrt{R_1(1 - l_{\mathrm{cav}})}\right)^2} \tag{2}$$

The discrepancy between the two accounts for the fact that a fraction $(1 - c_0)$ of the incident power is reflected at M1 due to mode-mismatch. Eq. 1 does not include the nonlinear loss term due to second harmonic generation, as this latter accounts for an additional loss of $\sim 10^{-4}$, which is negligible compared to the linear term. For this reason, the linear behaviour which is typically observed in second-harmonic generation crystals at high pump powers [18, 28, 29] is not appreciated in this case. Fig. 2 shows the measured UV power produced in the cavity setup (red dots) and the calculated power (dashed line) for a resonator with $l_{\mathrm{cav}} = 3.9 \times 10^{-3}$, which is consistent with the specified losses of our optical components as provided by the manufacturers. Based on this value, the coupling ratio for our setup was estimated to be $c_0 = 78\%$. Up to 250 µW of UV light are obtained at the maximum pump power of 15 mW at 507.4 nm. Fig. 3 (a) shows the far-field spatial profile of the UV beam after collimation, which is strongly affected by the BBO walk-off. Such an intensity profile is not suitable for DBT as its effect on the absorption linewidth of the atomic vapor cannot be modelled with the required accuracy. The mode quality was improved by strongly focusing the beam with a $f = 50$ mm lens. A 50 µm pinhole was placed at the beam waist and aligned using a 3-axes stage. About 20% of optical power is still available in the transmitted mode, which is enough for our application. Fig. 3 (b) shows the spatial profile measured in the far field after collimation with a $f = 200$ mm lens. The resulting beam shape can be more easily modelled so that its impact in the lineshape becomes negligible.

50% of the produced UV radiation is sent to a 60 µm^2 area SiC photodiode for detecting power variations. These are compensated by adjusting the RF power driving the AOM at 507.4 nm. Fig. 4 shows the power spectral density (top graph) and long-term behaviour (bottom graph) of the power fluctuations normalised to the average power in the carrier in an unstabilised (blue) and stabilised (red) condition. An increase in the noise is observed at about 20 kHz, which is due to frequency-to-power conversion in correspondence of the locking bandwidth of the cavity. The bandwidth of the intensity control loop is intentionally limited to 1 kHz to avoid cross-talk between the two. The 30% relative power variations observed on the system when the stabilisation is not active are reduced to 4×10^{-5} over timescales of few minutes, which is the typical duration of a full experimental session. On the long term, a residual effect of the air-conditioning system, which has a cycle time of about 1500 s, leads to maximum relative deviations from the nominal value of 1×10^{-4}. These performances fully meet the requirement for this experiment, as their impact on the absorption lineshape is already negligible, and could be further improved by passively insulating the system.

The operation of the UV source was verified by observing the shape of the intercombination transition for the ^{202}Hg bosonic isotope in a 20-mm-long spectroscopic cell sealed at the two ends by a pair of wedged AR-coated quartz windows and filled with Hg vapors, temperature-stabilized at the triple point of water to within 0.01 K. A SiC photodiode was used to measure the transmitted UV radiation while scanning the frequency of the NIR laser source by 2.5 GHz in about 1 s. Simultaneously, additional current was sent to the slave laser at 507.4 nm in a feed-forward scheme, so that injection from the seed light could be maintained throughout the full frequency scan. During the scan, we constantly measured the the NIR laser frequency on a wavemeter to confirm the absence of mode-hops on any of the stages. Fig. 5 shows an example of the absorption spectrum which can be obtained with a continuous scan. It shows the ^{202}Hg absorption profile along with a portion of the ^{200}Hg peak at higher frequency detuning, and the convolution of the ^{204}Hg transition and hyperfine structure components of the fermionic isotopes ^{199}Hg and ^{201}Hg at lower frequencies. A continuous and wider than 10 GHz scan of the UV laser frequency was possible without mode hops, while maintaining the single-mode emission. The mode-hop-free tunable range of the UV laser is currently limited by that of the master laser which is only 2.5 GHz, and could be further increased by applying the feed-forward approach also to the master laser current. Nevertheless, the achieved tunability is already enough for the aims of DBT.

In conclusion, we realised a laser source at 253.7 nm for DBT on the intercombination line of bosonic Hg isotopes with a target ppm accuracy on the absolute temperature determination from the absorption profile. The narrow linewidth regime can be reached by stabilising the 1014.8 nm laser to a narrow-linewidth laser in the IR, where this feature is readily achievable, using a frequency comb as a transfer oscillator. Fiber optical combs have sufficient power at both wavelengths to allow beatnotes detection with suitable signal-to-noise ratio. The UV laser source will then copy the spectral purity of the reference laser with a four-fold amplification in the noise due to the frequency upconversion. Furthermore, using the comb will provide a controlled frequency scan as required for achieving the target accuracy in the temperature determination.

The demonstrated features make our spectrometer suitable for primary gas thermometry on mercury vapours, providing an optical method for the practical realization of the new kelvin.

Funding

This work is funded by the Italian Ministry for Education and Research, under Project n. 20152MRAKH "A new primary method of gas thermometry based upon Doppler-broadened mercury spectroscopy in the UV region", PRIN2015 Call.

Disclosures

The use of trade names in this article is inserted for completeness and does not constitute an endorsement by the authors. The authors declare no conflicts of interest.

References

[1] G. Machin, Meas. Sci. Technol. **29**, 022001 (2018).

[2] B. Fellmuth, J. Fischer, G. Machin, S. Picard, P. Steur, O. Tamura, R. White, H. Yoon, Phil. Trans. R. Soc. A **374** 20150037 (2016).

[3] M. R. Moldover, R. M. Gavioso, J. B. Mehl, L. Pitre, M. de Podesta and J. T. Zhang, Metrologia **51**, 1 (2014).

[4] L. Pitre, F. Sparasci, L. Risegari, C. Guianvarch, C. Martin, M. E. Himbert, M. D. Plimmer, A. Allard, B. Marty, P. A. Giuliano Albo, B. Gao, M. R. Moldover and J. B. Mehl, Metrologia **54**, 856 (2017).

[5] Ch. Gaiser, Th. Zandt and B. Fellmuth, Metrologia **52**, 5 (2015).

[6] L. Gianfrani, Philos. Trans. R. Soc. A **374**, 20150047 (2016).

[7] A. Castrillo, E. Fasci, H. Dinesan, S. Gravina, L. Moretti, and L. Gianfrani, Physical Review Applied **11**, 064060 (2019).

[8] G.-W. Truong, E. F. May, T. M. Stace, and A. N. Luiten, Phys. Rev. A **83**, 033805 (2011).

[9] G.-W. Truong, J. D. Anstie, E. F. May, T. M. Stace, A. N. Luiten, Nat. Comm. **6**, 8345 (2015).

[10] J. J. McFerran, L. Yi, S. Mejri, S. Bize, Opt. Lett. **35**, 3078 (2010).

[11] H. Hachisu, K. Miyagishi, S. G. Porsev, A. Derevianko, V. D. Ovsiannikov, V. G. Pal'chikov, M. Takamoto, and H. Katori, Physical Review Letters **100**, 053001 (2008).

[12] M. Witkowski, G. Kowzan, R. Munoz-Rodriguez, R. Ciurylo, P. S. Z., P. Maslowski, M. Zawada, Opt. Expr. **27**, 11069 (2019).

[13] L. Hong-Li, Y. Shi-Qi, L. Kang-Kang, Q. Jun, X. Zhen, H. Tao, W. Yu-Zhu, Chinese Physics B **22**, 043701 (2013).

[14] P. Villwock, S. Siol, and Th. Walther, Europ. Phys. J. D **65**, 251 (2011).

[15] M. Horbatsch, E. A. Hessels, Phys. Rev. A **82**, 0521519-1-6 (2010).

[16] G. Almog, M. Scholz, W. Weber, P. Leisching, W. Kaenders, Th. Udem, Rev. Sci. Instrum. **86**, 033110 (2015).

[17] J. Alnis, U. Gustafsson, G. Somesfalean, and S. Svanberg, Appl. Phys. Lett **76**, 1234 (2000).

[18] M. Scheid, F. Markert, J. Walz, J. Wang, M. Kirchner, and T. W. Haensch, Opt. Lett. **32**, 955 (2007).

[19] D. Akamatsu, M. Yasuda, T. Kohno, A. Onae, F.-L. Hong, Opt. Expr. **19**, 20476-2051 (2011)

[20] N. Chiodo, F. Du Burck, J. Hrabina, Y. Candela, J.-P. Wallerand, O. Acef, Opt. Commun. **311**, 239 (2013).

[21] C. J. H. Pagett, P. H. Moriya, R. Celistrino Teixeira, R. F. Shiozaki, M. Hemmerling, and Ph. W. Courteille, Rev. Sci. Instr. **87**, 053105 (2016).

[22] T. Hosoya, M. Miranda, R. Inoue, M. Kozuma, Rev. Sci. Instr. **86**, 073110 (2015).

[23] Y. Shimada, Y. Chida, N. Ohtsubo, T. Aoki, M. Takeuchi, T. Kuga, Y. Torii, Rev. Sci. Instr. **84**, 063101 (2013).

[24] G. D. Boyd and D. A. Kleinman, J. Appl. Phys. **39**, 3597 (1968).

[25] T. Freegarde and C. Zimmermann, Opt. Commun. **199**, 435 (2001)

[26] W. P. Risk, T. R. Gosnell, and A. V. Nurmikko, Compact Blue-Green Lasers (Cambridge University, 2003)

[27] T. Haensch and B. Couillaud, Opt. Commun. **35**, 441 (1980)

[28] M. Pizzocaro, D. Calonico, P. Cancio Pastor, J. Catani, G. A. Costanzo, F. Levi, L. Lorini, Appl. Opt. **53**, 3388 (2014).

[29] R. Steinborn, A. Koglbauer, P. Bachor, T. Diehl, D. Kolbe, M. Stappel, J. Walz, Opt. Expr. **21**, 22693 (2013)

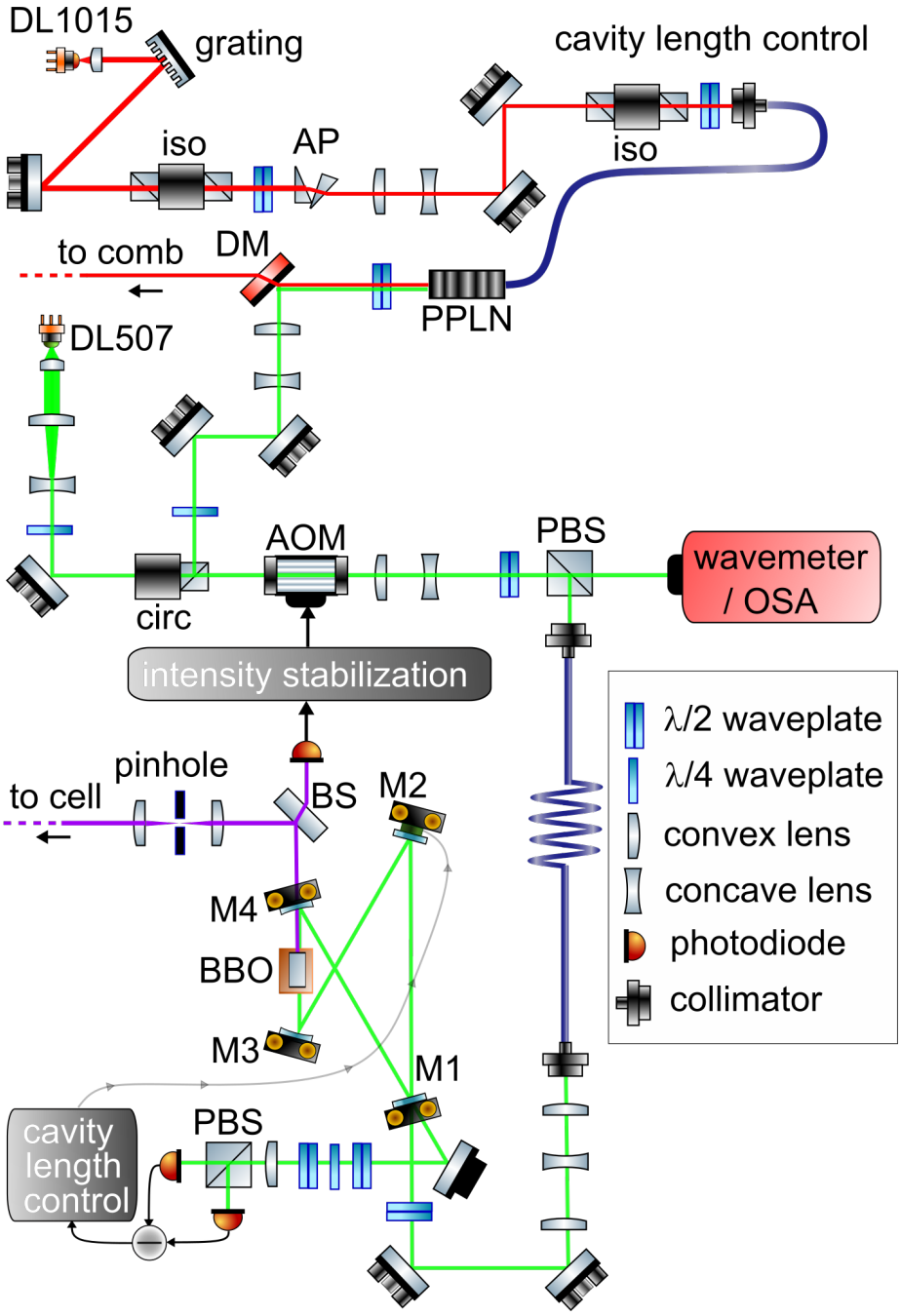

Figure 1: A sketch of the optical setup. DL1015: master laser at 1014.8 nm; iso: isolators; AP: anamorphic prisms; PPLN: crystal for first-stage duplication; DM: dichroic mirror; circ: circulator; DL507: slave diode laser at 507.4 nm; AOM: acusto-optic modulator; (P)BS, (polarization) beam splitter; OSA: optical spectrum analyzer; M1: input mirror for second-stage duplication cavity; M2: piezo-actuated mirror; M3, M4: concave mirrors; BBO: crystal for second-stage duplication.

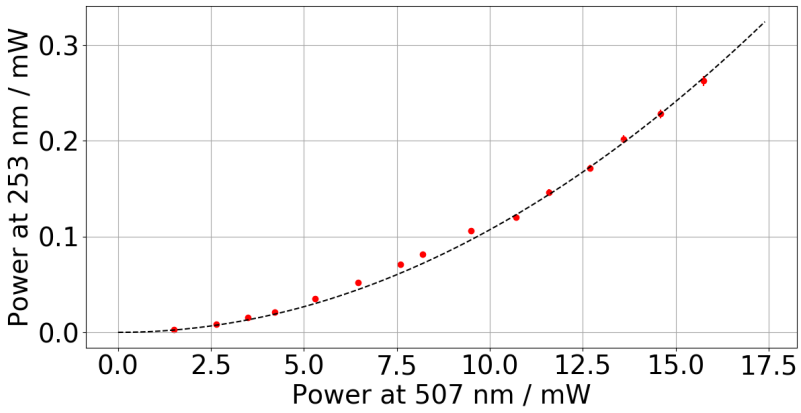

Figure 2: Red points: measured power at 253.7 nm produced in a cavity setup as a function of pump power at 507.4 nm. Dashed line: calculated power for a resonator with $l_{\mathrm{cav}} = 3.9 \times 10^{-3}$ and $c_0 = 78\%$.

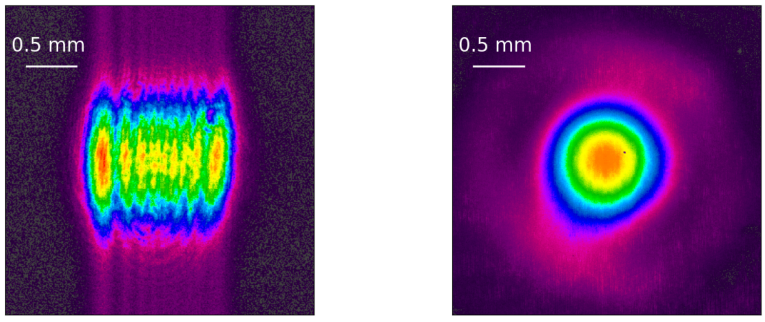

Figure 3: Left: spatial profile of the UV beam as it exits the cavity. Right: spatial profile when a mode-cleaning stage is added.

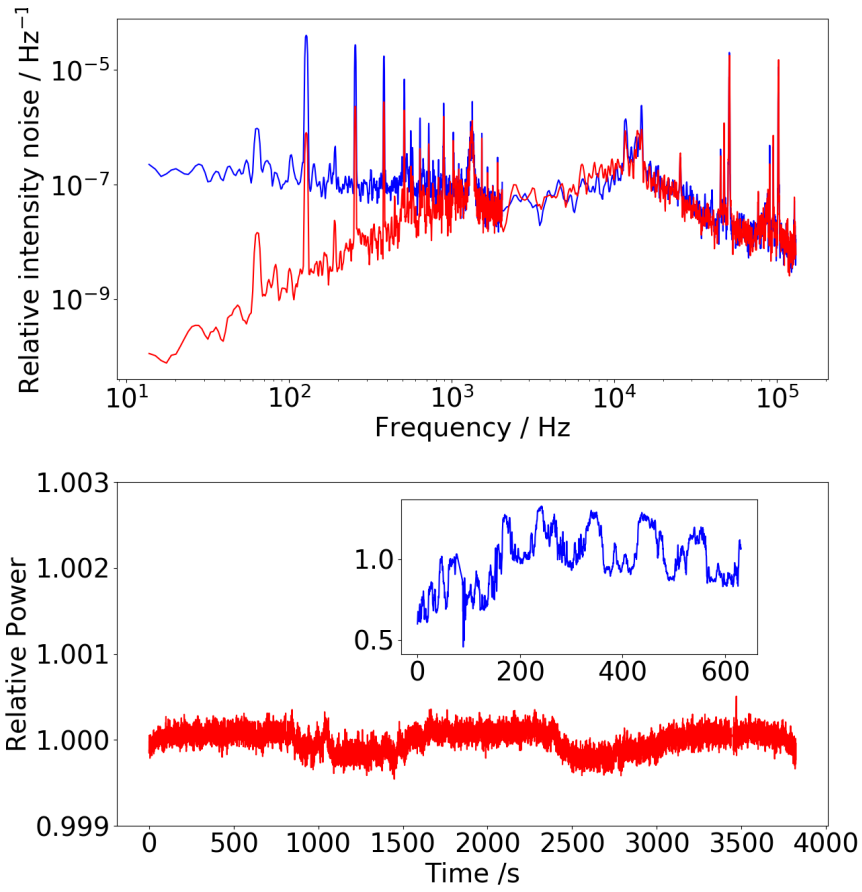

Figure 4: Top: power spectral density of the relative intensity noise at 253.7 nm in an unstabilised (blue) and stabilised (red) condition. Bottom: long-term power variations normalised to the average power in a stabilised (red) and unstabilised (inset, blue) condition.

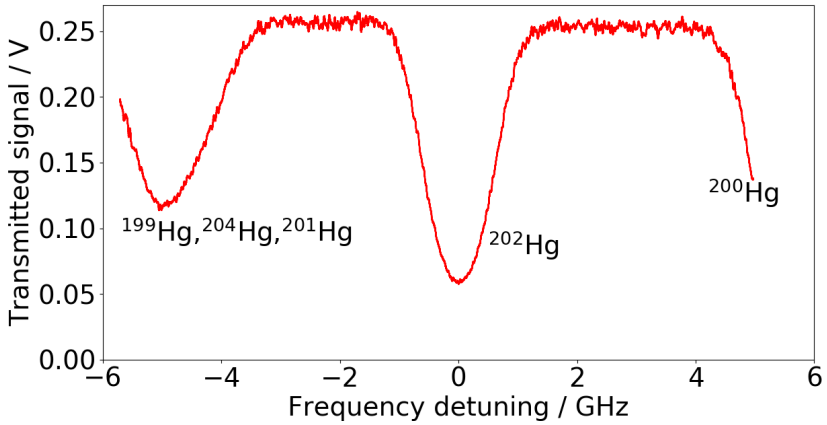

Figure 5: Absorption spectrum of the Hg cell across the ^{202}Hg intercombination line.